# A theoretical model on coupled fluid–structure impact buckling

**Qingjie Zhang**

*Department of Engineering Mechanics, Wuhan University of Technology, Wuhan, People's Republic of China*

**Qinghua Qin**

*Department of Mechanics, Huazhong University of Science and Technology, Wuhan, People's Republic of China*

**Jianzhong Wang**

*Department of Mechanical Engineering, Wuhan University of Technology, Wuhan, People's Republic of China*

*A model simulating a coupled fluid–structure impact buckling phenomenon is constructed in this paper. Based on the experiment[1,2] the model is designed as an impact system in which a small imperfection elastoplastic column is attached by its upper end to a large mass and by its lower end to a flat plate; it then perpendicularly impacts a viscous water free surface from a certain drop height or in a certain falling velocity. A one-dimensional compressible inviscid air layer is assumed to exist between the plate and the water free surface. A coupled transversely flexural vibration is induced in the column when the hydrodynamic slamming between the plate and the water occurs during the impact. A mathematical description is given for the model with three sets of coupled dynamic equations: a nonlinear finite element and the Prandtl–Reuss plastic theory are applied to the structure, the one-dimensional continuity and momentum equations of a compressible inviscid fluid are applied to the air, and the two-dimensional Navier–Stokes equations of an incompressible viscous fluid are applied to the water. In numerical analysis, the three sets of coupled equations are first decomposed by a staggered iteration method and then solved by an extended Wilson-0 time integration scheme and a finite difference method. To verify the suitability of the model, two numerical examples are calculated in the paper: one is a calculation of the relationship between the column's slenderness and the hydrodynamic slamming duration, and the other is a calculation of the column's critical impact values. The numerical results are compared with the corresponding experimental ones. The comparison demonstrates that the present model is capable of simulating a coupled dynamic buckling phenomenon that can occur in fluid-structure impact engineering.*

**Keywords:** dynamic buckling, fluid-structure impact buckling, hydrodynamic slamming, impact engineering

## Introduction

In some water–structure impact engineering (such as ship structure–water slamming and impacting of a flying slender body against water), one may encounter a new dynamic buckling phenomenon distinct from that of vibration buckling,[3] pulse buckling,[4] and dynamic snap-through buckling.[5] Recently, one of the authors of this paper studied this new buckling phenomenon.[1,2] The experiments involved a series of impact buckling tests for columns, columns with elastic supports, and plates. In these tests, the structural members are axially loaded by a special test rig in which they are attached by their upper end to a large mass and by their lower end to a flat plate; then they perpendicularly impact the free

Address reprint requests to Professor Zhang at the Department of Engineering Mechanics, Wuhan University of Technology, 14 Luoshi Rd., Wuhan #430070, People's Republic of China.

Received 16 October 1991; revised 27 May 1992; accepted 8 June 1992.

surface of a water field from different drop heights. The buckling phenomenon is simulated during the impact when the hydrodynamic slamming between the plate and the water takes place. The term coupled fluid-structure impact buckling was used by the authors because of the relationship between the structural response and the water impact.

Fluid–structure impact buckling has two basic characteristics as revealed by the experimental study: (a) the structures may experience three critical states of buckling, postbuckling, and plastic collapse in one impact, each of the states corresponding to a particular transition in the structural dynamic response; (b) there exists a coupling between the structural buckling and the hydrodynamic slamming. For the coupling, when the structures produce large deformation during the postbuckling and plastic collapse, a distortion phenomenon can be observed in the slamming pulse shape. The two characteristics distinguish fluid–structure impact buckling from known buckling phenomena in two respects: (a) the new phenomenon has three critical states and each state has a particular definition which differs from those of the known phenomena's critical states; (b) the fluid–structure impact buckling can not be treated as a buckling problem with prescribed axial loading due to the coupling between the structural deformation and the deformation of the water free surface. With special emphasis on the differences from other buckling phenomena, definitions for fluid–structure impact buckling have been suggested by the experimental study.[1,2]

To provide a general understanding of the new buckling phenomenon, the present work proposes a theoretical model that describes the two basic characteristics. On the basis of the experiments,[1,2] the model is constructed as an impact system in which a small imperfection elastoplastic column is attached by its upper end to a large mass and by its lower end to a flat plate; it then perpendicularly impacts a free surface of an incompressible viscous water field from a certain drop height or in a certain falling velocity. To verify the suitability of the model, two numerical examples are considered: One is a calculation of the relationship between the column's slenderness and the hydrodynamic slamming duration; the other is a calculation of the column's critical impact values. The numerical results are compared with the corresponding experimental ones. The comparison demonstrates that the proposed model is an acceptable one for describing the new buckling phenomenon.

## Model and mathematical description

As described in the introduction, the model simulating the fluid–structure impact buckling phenomenon is shown in *Figure 1*. Between the plate and the water free surface, a one-dimensional inviscid compressed air layer is assumed to exist during the impact. The column has two possible boundary conditions at its two ends: simply supported and clamped. The clamped boundary condition is indicated in the figure.

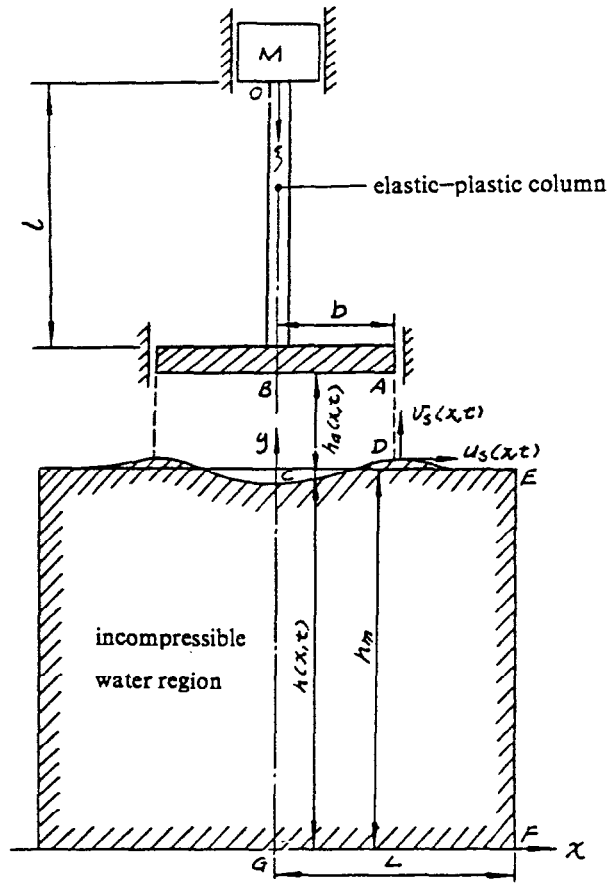


**Figure 1.** A model simulating fluid–structure impact buckling.

In what follows, the mathematical description of the model is given with three sets of coupled motion equations for the air, water, and structure.

## The structural motion equation

Assume no initial deformation and stress exist in the column before the water–plate slamming takes place; thus the buckling of the column is caused only by the hydrodynamic slamming pressure. By denoting the compression, deflection, stress, membrane force, and bending moment at the location $\xi$ and time $t$ in the column with $u^c(\xi,t)$, $u^b(\xi,t)$, $\sigma(\xi,t)$, $N^c(\xi,t)$, and $N^b(\xi,t)$, respectively, the buckling equation that governs the motion of the mass-column-plate unit can be expressed in terms of the virtual work principle as follows:

$$\int_1 \{\delta U\}^T \rho_s^* \{\ddot{U}\}\, d\xi + \int_1 \{\delta\chi\}^T \{N\}\, d\xi + \int_1 \{\delta U\}^T \{\underline{N}\}\, d\xi + \{\delta \underline{U}\}^T \{\underline{N}\} + \{\delta \underline{U}\}[\underline{M}]\{\ddot{\underline{U}}\} = \{\delta \underline{U}\}^T \{\underline{R}\} \tag{1}$$

Where $\{U\} = [u^c, u^b]^T$, $\{\chi\} = [\chi^c, \chi^b]^T$, $\{N\} = [N^c, N^b]^T$

$\{\underline{U}\} = [u_0^c, u_1^c]^T$, $u_0^c = u^c(0,t)$, $u_1^c = u^c(1,t)$

$\{\underline{N}\} = [\rho_s^*(g - \beta_2 N_0^c), 0]^T$, $N_0^c = N^c(0,t)$

$\{\underline{N}\} = [-N_0^c, \beta_1 N_0^c]^T$

$$\{\underline{M}\} = \begin{pmatrix} M & 0 \\ 0 & m \end{pmatrix}$$

$$\{\underline{R}\} = \left[0, 2a \int_0^b P_a(x,t)\, dx\right]^T$$

$$\chi^c = \frac{\partial u_c}{\partial \xi} + \frac{1}{2}\left(\frac{\partial u^b}{\partial \xi}\right)^2, \quad \chi^b = \frac{\partial^2 u^b}{\partial \xi^2}$$

$$N^c = \int_A \sigma dA, \quad N^b = \int_A -\eta\sigma dA$$

Other symbols in the expressions are given in the nomenclature.

To treat the plasticity spreading along the column's length and over the cross-section thickness, it is convenient to divide the spatial domain in equation (1) by a finite element method. By using the $C(0)$ Lagrange and $C(1)$ Hermitan beam elements for the discretization of $u^c$ and $u^b$, respectively, $\{U\}$ and $\{\chi\}$ in (1) can be expressed in a finite element form as[6,7]

$$\{dU\} = [\bar{N}]\{d\delta\}^e \text{ and } [\bar{N}] = \begin{bmatrix} [\bar{N}^m] & 0 \\ 0 & [\bar{N}^b] \end{bmatrix} \tag{2}$$

$$\{d\chi\} = [\bar{B}]\{d\delta\}^e \text{ and } [\bar{B}] = \begin{bmatrix} [B_L^m] & [B_{NL}^m] \\ 0 & [B_L^b] \end{bmatrix} \tag{3}$$

where $[\bar{N}^m]$ and $[\bar{N}^b]$ are the membrane and bending shape function matrices of the beam element, respectively; $[B_L^m]$, $[B_L^b]$, and $[B_{NL}^m]$ are the linear membrane strain matrix, linear bending strain matrix, and nonlinear strain matrix, respectively; $\{\delta\}^e$ is the nodal point displacement vector in an element.

By substituting equations (2) and (3) into equation (1), (1) can be expressed in the form of a finite element as

$$[M]\{\ddot{\delta}\} + \{F\} = \{R\} \tag{4}$$

where $\{\ddot{\delta}\}$ is the nodal point acceleration vector of the finite element assemblage; $[M]$ is the mass matrix of the assemblage, including the contributions of $\int_0^l [\bar{N}]^T \rho_s^* [\bar{N}] d\xi$ and $[\underline{M}] = \begin{bmatrix} M & 0 \\ 0 & m \end{bmatrix}$; $\{F\}$ is the nodal point internal force vector of the finite element assemblage, including the contributions of $\int_0^l [\bar{B}]^T \{N\} d\xi$, $\int_0^l [\bar{N}]^T \{\underline{N}\} d\xi$ and $\{\underline{N}\}$; $\{R\}$ is the nodal point external load vector of the finite element assemblage, and $\{R\} = [0, 0, 0, \cdots 0, 2a\int_0^b P_a(x,t)dx]^T$.

Because no initial deformation and stress exist in the column before the slamming pressure is built, the initial boundary conditions of the column are given by

$$\begin{aligned} u^c(\xi,0) &= 0 \qquad \dot{u}^c(\xi,0) = 0 \\ u^b(\xi,0) &= w(\xi) \qquad \dot{u}^b(\xi,0) = \bar{w}(\xi) \end{aligned} \tag{5a}$$

and

$$u^c(0,t) = u_0^c(t) \qquad u^c(l,t) = u_l^c(t)$$

$$u^b(0,t) = \frac{\partial u^b(0,t)}{\partial \xi} = u^b(l,t) = \frac{\partial u^b(l,t)}{\partial \xi} = 0 \tag{5b}$$

where $w(\xi)$ and $\bar{w}(\xi)$ are the initial transverse displacement and velocity disturbances, respectively.

*The air and water motion equations*

The plate–water impact in the model is an important hydrodynamic phenomenon. A problem similar to this phenomenon has been investigated by Chuang,[8,9] Verhagen,[10] and Koehler,[11] among others. By referring to *Figure 2* and Koehler's work, below we give the air and water motion equations separately.

The air motion equation

$$\frac{\partial}{\partial x}(\rho_a u_a h_a) + \frac{\partial}{\partial t}(\rho_a h_a) = 0 \tag{6a}$$

$$\frac{\partial u_a}{\partial t} + u_a \frac{\partial u_a}{\partial x} = -\frac{1}{\rho_a}\frac{\partial P_a}{\partial x} \qquad 0 \le x \le b \tag{6b}$$

$$\frac{p_a}{\rho_a} = k = \frac{P_{\text{atm}}}{\rho_{\text{atm}}} \tag{6c}$$

$$\frac{\partial}{\partial t} h_a(x,t) = -V(t) - v_s(x,t) \tag{6d}$$

$$u_a(x,t) = \frac{h_a(b,t) \cdot u_a(b,t)}{h_a(b,t) + (x-b)tg\dfrac{\beta}{2}} \qquad x \ge b \tag{6e}$$

with initial condition:

$$P_a(x,0) = P_{\text{atm}}, u_a(x,0) = -\frac{x}{h_a(x,0)} \cdot \frac{\partial}{\partial t} h_a(x,0) \tag{6f}$$

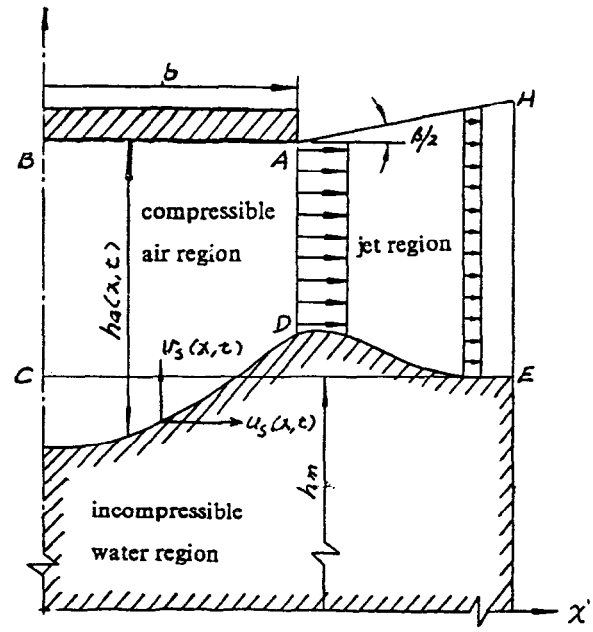


**Figure 2.** Compressible air region detail.

and boundary condition:

$$u_a(0,t) = 0, P_a(b,t) = P_{atm} \tag{6g}$$

where $u_a$, $P_a$, and $\rho_a$ are the air velocity in the $x$-direction, pressure (absolute), and density, respectively; $V(t)$ and $v_s(x,t)$ are the falling plate velocity and the free-surface water velocity in the $x$-direction, respectively; $h_a$ is the air layer thickness. Other symbols are referred to in the nomenclature.

The water motion equation[11]

$$\frac{\partial u}{\partial x} + \frac{\partial v}{\partial y} = 0 \tag{7a}$$

$$\rho\left(\frac{\partial u}{\partial t} + u\frac{\partial u}{\partial x} + v\frac{\partial u}{\partial y}\right) = -\frac{\partial P}{\partial x} \tag{7b}$$

$$\frac{\partial^2 P}{\partial x^2} + \frac{\partial^2 P}{\partial y^2} = -Q \tag{7c}$$

$$Q = \rho\left[\left(\frac{\partial u}{\partial x}\right)^2 + 2\left(\frac{\partial v}{\partial x}\right)\left(\frac{\partial u}{\partial y}\right) + \left(\frac{\partial v}{\partial y}\right)^2\right] \tag{7d}$$

with initial condition:

$$P(x,y,0) = P_{Hs}, u(x,y,0) = 0, v(x,y,0) = 0 \tag{7e}$$

and boundary condition:

on CG

$$\left.\frac{\partial P(x,y,t)}{\partial x}\right|_{x=0} = 0, u(0,y,t) = 0, \left.\frac{\partial v(x,y,t)}{\partial x}\right|_{x=0} = 0 \tag{7f}$$

on CD

$$P(x,h,t) = P_a, u(x,h,t) = u_s, v(x,h,t) = v_s \tag{7g}$$

on DE

$$P(x,h,t) = P_{atm}, u(x,h,t) = u_s, v(x,h,t) = v_s \tag{7h}$$

on GF

$$\left.\frac{\partial P(x,y,t)}{\partial y}\right|_{y=0} = -\rho g, u(x,0,t) = 0, v(x,0,t) = 0 \tag{7i}$$

on EF

$$\left.\frac{\partial P(x,y,t)}{\partial x}\right|_{x=L} = -\rho\left(\frac{\partial u}{\partial t} + \frac{\partial u}{\partial x} + v\frac{\partial u}{\partial y}\right)\Bigg|_{x=L}$$

$$\left.\frac{\partial u(x,y,t)}{\partial x}\right|_{x=L} = -\left.\frac{\partial v(x,y,t)}{\partial y}\right|_{x=L} \tag{7j}$$

$$\left.\frac{\partial v(x,y,t)}{\partial x}\right|_{x=L} = 0$$

Moreover, on the air–water interface, the free-surface water velocity $u_s$ is related to the air velocity $u_a$. This relationship is

$$u_s = 0.198[u_a^{1.20}\rho_a^{0.533}\mu_a^{0.133}v^{0.333}x^{0.20}]/\mu^{0.667} \tag{7k}$$

In the above expressions, $u$ and $v$ are the water velocities in $x$ and $y$ directions, respectively; $P$ and $\rho$ are the water pressure (absolute) and density, respectively; $u_s$ and $v_s$ are the free-surface water velocities in $x$ and $y$ directions, respectively. Other symbols are referred to in the nomenclature.

*Peak impact and treatment after peak impact*

It has been indicated[1,2] that the hydrodynamic slamming pulse is essentially a semi-sine wave before the column's postbuckling and plastic collapse take place. A typical record for the slamming pulse from the experiment is shown in *Figure 3* where $\epsilon_c$, $t_p$, and $t_0$ are the slamming peak value, peak slamming time, and slamming duration, respectively. The experiment demonstrates that $\epsilon_c$ rises with increasing slamming height and $t_0$ varies with column slenderness: the smaller the slenderness, the shorter the $t_0$. For a prescribed slenderness, however, $t_0$ is basically unchanged provided that the column does not display postbuckling and plastic collapse in one impact.

For a theoretical study, however, when does the peak impact occur and how can it be determined? The answer to this question may lead to a simplified treatment for the present model analysis. From the studies by Chuang,[9] Verhagen,[10] and Koehler,[11] the peak impact is considered to occur at the instant the deformed water free surface makes contact with the edge of the plate. According to this peak impact condition, $t_p$ in *Figure 3* coincides with the time the plate's edge touches the deformed water free surface. On the other hand, equations (6a)–(7k) are valid until the deformed water free surface makes contact with the plate's edge. Thus, (6a)–(7k) constitute the mathematical description of the air and water motion in the phase of $0 \le t \le t_p$.

To obtain the decay phase of the slamming pulse, the mathematical description of the air and water motion after the peak impact is needed. However, this description is not always necessary. It is known from the experiment that there is no distortion phenomenon in the slamming pulse shape before the column's postbuckling and plastic collapse take place. Therefore, if only the buckling criterion is required rather than all the criteria

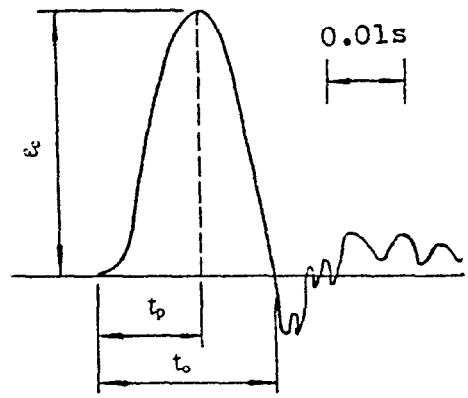


**Figure 3.** A typical fluid–structure slamming pulse.

including the postbuckling and plastic collapse, a simplified treatment for the model analysis is possible since the decay phase of the slamming pulse can be estimated in this case from the rise phase. The simplification procedure is (a) to divide the motion of the model into two phases: $0 \le t \le t_p$ and $t > t_p$; (b) for $0 \le t \le t_p$, to describe the motion with equations (1)–(7k); (c) for $t > t_p$, to define the motion of the column remaining with the description in the section outlining the structural motion equation except the initial condition, but the slamming pressure in this phase is treated as a prescribed load and estimated from the preceding phase (i.e., the rise portion of the pulse). In this simplification, the motion description of the air and water in $t > t_p$ is omitted, and the column's motion is considered to be independent of the air and water behavior.

In this paper, we restrict our attention to the buckling criterion and the relationship between the peak impact time and the column slenderness. Therefore, we use the simplification procedure in this analysis.

## Solution of mathematical equations

It is obvious from the mathematical description given previously that the column, air, and water motion equations are three sets of coupled ones. It is seen that equation (4) contains an unknown pressure $p_a$, which is related to the water–plate hydrodynamic slamming. On the other hand, the air equation (6d) involves an unknown quantity $V$, the falling velocity of the plate. Between the air and water, their behaviors are coupled through the air equation (6d), which includes the free-surface water velocity $v_s$ and the water equation (7g), which contains the air pressure $p_a$ and air velocity $u_a$.

Because of the coupling among the three sets of motion equations, they are difficult to solve directly. In what follows, we first introduce a decomposition procedure for these equations. Once these equations are decomposed by the procedure, their solutions can be obtained by some appropriate numerical methods.

### *Decomposition of the coupled equations*

Before the decomposition of the coupled equations is started, it is useful to review the coupling characteristics. It is found from the air description that except (6d), which gives a relationship between $h_a$, $V$, and $v_s$, the remaining equations have no explicit connection with the water and structural equations. Thus if $h_a$ can be predetermined independently of the other quantities, the air description will be separated from the water and structural equations. Moreover, since there is no direct connection between the structural and water equations, these two sets of equations can be treated separately after the air description is decomposed.

The above discussion suggests a possible decomposition procedure for the coupled equations. The key point of the procedure is to give an appropriate estimation for the air thickness $h_a$ in advance. Usually this is difficult. However, when the coupling characteristics are combined with a special iteration technique, the difficulty can be surmounted.

Below, we start the decomposition procedure. We first divide the time domain $0 \le t \le t_p$ by the discrete time points $t_j = t_{j-1} + \Delta t\,(j = 1, 2, \ldots J)$, where $\Delta t = t_p/J$ is the time step length from $t_{j-1}$ to $t_j$ and $J$ is a prescribed number for the total time steps. Then we assume that the quantities at the time $t_{j-1}$, such as $h_a(x,t_{j-1})$, $V(t_{j-1})$, and $v_s(x,t_{j-1})$, are known. Our goal is to decompose the coupled equations defined at the time $t_j$. The decomposition procedure consists of the following steps:

Step 1. Estimate an appropriate value for $h_a(x,t_j)$ from equation (6d) and $h_a(x,t_{j-1})$, $V(t_{j-1})$, and $v_s(x,t_{j-1})$. This value is used as $h_a^0$, the first approximation of $h_a(x,t_j)$.

Step 2. Substitute $h_a^0$ into the remaining air equations and separate them from the water and structural ones.

Step 3. Solve the separated air equations for $u_a^0$ and $P_a^0$, which are the first approximations for $u_a(x,t_j)$ and $p_a(x,t_j)$, respectively.

Step 4. Substitute $h_a^0$, $u_a^0$, and $P_a^0$ into the water and structural equations respectively; thus these two sets of equations are decomposed.

Step 5. Solve the decomposed structural equations for ${}^0u^c$, ${}^0u^b$, ${}^0N^c$, ${}^0N^b$, and $V^0$, which are the first approximations of $u^c(\xi,t_j)$, $u^b(\xi,t_j)$, $N^c(\xi,t_j)$, $N^b(\xi,t_j)$, and $V(t_j)$, respectively.

Step 6. Solve the decomposed water equations for $u^0$, $v^0$, $v_s^0$, and $P^0$, which are the first approximation of $u(x,t_j)$, $v(x,t_j)$, and $p(x,t_j)$, respectively.

Step 7. From (6d) and the current values of $h_a^0$, $V^0$, and $v_s^0$, calculate the updated air thickness $h_a^1$.

Step 8. Identify whether or not the inequality $|h_a^1 - h_a^0| < \gamma$ holds true, where $\gamma$ is a positive value less than unity. If the inequality is true, add next time step to $t_j$, then repeat steps 1–7. Otherwise replace $h_a^0$ with $h_a^1$, then continue steps 2–7 until the inequality operates.

The above decomposition procedure is shown in *Figure 4*. It is seen from the figure that the procedure is in fact a staggered iteration technique.

### *Solution of the decomposed equations*

We now treat the three sets of decomposed equations. From the decomposed equations (6a) and (6b), it is found that if they are expressed in a proper finite difference form, an explicit solution scheme for $u_a$ and $p_a$ can be obtained. This is also true for the decomposed equations (7a) and (7b). Moreover, once $u$ and $v$ are calculated from their explicit solution schemes, the source term $Q$ in (7c) can be estimated independently of the pressure $p(x,y,t_j)$, and the pressure equation becomes a linear one. Thus, the solution of the pressure equation also becomes quite easy.

Based on the above discussion, a finite difference method is used in this paper to solve the decomposed air and water equations. The present method is identical to that used by Koehler[11] in his analysis of the plate–water hydrodynamic impact; therefore, its details are omitted here.

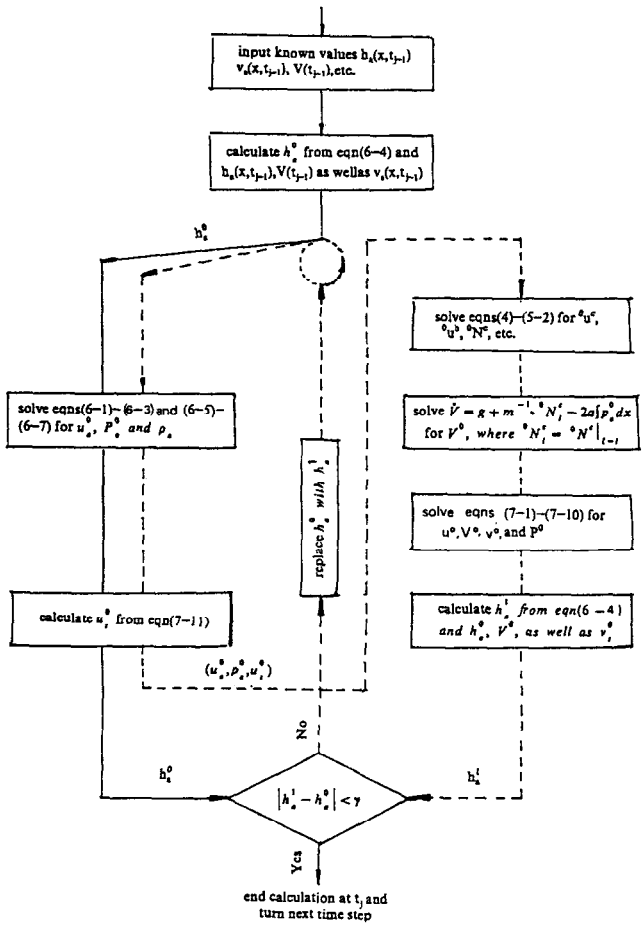


**Figure 4.** A staggered decomposition procedure for fluid–structure impact buckling.

For the solution of the decomposed equation (4), a tangential stiffness method with the Wilson-$\theta$ time integration scheme[12,13] is utilized in this paper. This method has been adopted by one of the present authors to treat a dynamically loaded stiffened plate subjected to both geometric and material nonlinearities.[7] When the method is used in the present problem, the center is to calculate the tangential stiffness matrix $[\hat{K}]$. According to Ref. 7, the tangential stiffness matrix $[\hat{K}]$ in this case is defined as

$$\{\Delta F\} = [\hat{K}_T]\{\Delta\delta\}, \{\Delta F\} = \{F\}^{t+\theta\Delta t} - \{F\}^t, \{\Delta\delta\} = \{\delta\}^{t+\theta\Delta t} - \{\delta\}^t \quad (8)$$

Where $[\hat{K}]$ is the tangential stiffness matrix at the time $t$; $\{\Delta\delta\}$ and $\{\Delta F\}$ are the nodal point displacement and internal force increments, respectively, from the time $t$ to $t+\theta\Delta t$, $\theta$ and $\Delta t$ being the Wilson's parameter and the time step length in the time integration scheme.

By substituting the expression of $\{F\}$ in equation (4) into equation (8) and using the following definitions

$$[B_L^m]_0 = [B_L^m]_{\xi=0}, [B_{NL}^m]_0 = [B_{NL}^m]_{\xi=0}, [B_L^b]_0 = [B_L^b]_{\xi=0} \quad (9)$$

$$[D_{ep}^m]_0 = [D_{ep}^m]_{\xi=0}, [D_{ep}^b]_0 = [D_{ep}^b]_{\xi=0}, [D_{ep}^{m,b}]_0 = [D_{ep}^{m,b}]_{\xi=0} \quad (10)$$

$$\{dN\} = \begin{bmatrix} [D_{ep}^m] & [D_{ep}^{m,b}] \\ [D_{ep}^{b,m}] & [D_{ep}^b] \end{bmatrix} \{d\chi\} \quad (11)$$

the tangential stiffness matrix is derived in this case as

$$[\hat{K}_\tau] = [\bar{K}_\tau] + [\tilde{K}_\tau] + [K_\tau] \quad (12a)$$

where

(a) $[\bar{K}_\tau] = \{\bar{F}\}\cdot\{\underline{F}\}$, $\{\bar{F}\}$ being the global structural vector of the finite element assemblage by $\{\bar{F}\}^e = \int_{le}[\bar{N}]^\tau\cdot[-\rho_s^*\cdot\beta_2, 0]^\tau\,d\xi$ and $\{\underline{F}\}$ being equal to

$$\{\underline{F}\} = [[D_{ep}^m]_0\cdot[B_L^m]_0, [D_{ep}^m]_0\cdot[B_{NL}^m]_0 + [D_{ep}^{m,b}]_0\cdot[B_L^b]_0, 0, 0, \cdots 0] \quad (12b)$$

(b) $[\tilde{K}_\tau] = \{\tilde{F}\}\cdot\{\underline{F}\}$, $\{\tilde{F}\}$ being equal to

$$\{\tilde{F}\} = [-1, 0, 0, \cdots 0, \beta_1, 0, 0, \cdots 0]^\tau \quad (13)$$

(c) $[K_\tau] = \Sigma_e [K_\tau]^e$, $e$ being the total finite element number and $[K_\tau]^e$ being calculated by

$$[K_\tau]^e = \begin{bmatrix} [K_L^m] & [K_{NL}^{m,b}] \\ [K_{NL}^{b,m}] & [K_o^b] + [K_L^b] + [K_{NL}^b] + [K_{L,NL}^b] + [K_{L,NL}^b]^T \end{bmatrix} \quad (14)$$

in which the submatrices are defined as

$$[k_o^b] = \int_{le}\left(\frac{d[\bar{N}^b]^T}{d\xi}\right)N^c\left(\frac{d[\bar{N}^b]}{d\xi}\right)d\xi \quad (15)$$

$$[K_L^b] = \int_{le}[B_L^b]^T[D_{ep}^b][B_L^b]\,d\xi \quad (16)$$

$$[K_{NL}^b] = \int_{le}[B_{NL}^m]^T[D_{ep}^m][B_{NL}^m]\,d\xi \quad (17)$$

$$[K_L^m] = \int_{le}[B_L^m]^T[D_{ep}^m][B_L^m]\,d\xi \quad (18)$$

$$[K_{NL}^{m,b}] = \int_{le}[B_L^m]^T[D_{ep}^m][B_{NL}^m]\,d\xi + \int_{le}[B_{NL}^m]^T[D_{ep}^{m,b}][B_L^b]\,d\xi \quad (19)$$

In these expressions, $[D_{ep}^m]$, $[D_{ep}^b]$, and $[D_{ep}^{m,b}]$ are the column's membrane, bending, and membrane-bending elastioplastic matrices, respectively. These matrices have been defined in Ref. 7.

Once $[\hat{K}_\tau]$ is determined from equations (11)–(19), the response of the decomposed nonlinear equation (4) is easily obtained by the solution of its linearized form as

$$[M]\{\ddot{\delta}\}^{t+\theta\Delta t} + [\hat{K}_T]^t\{\Delta\delta\} = \{R\}^{t+\theta\Delta t} - \{F\}^t \quad (20)$$

where $\{R\}^{t+\theta\Delta t}$ is the nodal point external force at the time $t + \theta\Delta t$.

## Impact criteria and numerical examples

In this section, we will analyze two numerical examples with the present theoretical model. One of the examples is a calculation of the relationship between the peak impact time $t_p$ and the column's slenderness ratio $\lambda$; the other is a calculation of the column's critical values. The common parameters used in the two examples are given below

$$L = 3.0\,m, h_m = 3.0\,m, a = 0.4\,m, b = 0.4\,m$$
$$\rho = 999.6\,\text{kg/m}^3, \mu = 1.19 \times 10^{-9}\,\text{Ns/m}^3$$
$$P_{\text{atm}} = 101.36\,\text{K Pa}, \rho_{\text{atm}} = 1.20\,\text{kg/m}^3$$
$$\mu_{\text{air}} = 1.77 \times 10^{-5}\,\text{Ns/m}^2$$
$$M = 1000.0\,\text{kg}, m = 80.0\,\text{kg}, g = 9.80\,\text{m/s}^2$$
$$\rho_s = 7.8 \times 10^3\,\text{kg/m}^3, \sigma_y = 2.6264 \times 10^8\,\text{N/m}^2$$
$$E = 2059.96 \times 10^8\,\text{N/m}^2, H' = 0.0$$

*Example 1. Calculation on the* $t_p$ *vs.* $\lambda$ *curve*

Four columns with a clamped boundary condition and a rectangular cross-section are calculated in this example. The geometry of the columns is $b_s \times h_s \times 1$, where 1 = 0.3 m, 0.4 m, 0.5 m, and 0.6 m is the length of the columns, $b_s = 14 \times 10^{-3}$ m and $h_s = 8.0 \times 10^{-3}$ m are the cross-section width and thickness, respectively. The three columns with the lengths of 0.4 m, 0.5 m, and 0.6 m are the same as those used in the experimental study, namely the specimens s11, s21, and s31 in Refs. 1 and 2. The initial condition of the columns is assumed to be

$$u^c(\xi,0) = \dot{u}^c(\xi,0) = \dot{u}^b(\xi,0) = 0 \tag{21}$$

$$u^b(\xi,0) = 16w_0 \cdot \frac{\xi^2}{\iota^2} \cdot \left(1 - 2\frac{\xi}{\iota} + \frac{\xi^2}{\iota^2}\right) \tag{22}$$

Where $w_0$ is the initial transverse displacement disturbance at the center, its value is taken as $1.0 \times 10^{-3}$ m. This value is close to those of s11, s21, and s31.

The initial air thickness is chosen in this example as $h_a(x,0) = 0.2\ m$.

For each of the considered columns, the peak impact time $t_p$ is calculated from the present model. The results are plotted in *Figure 5* against the slenderness ratio $\lambda$. From this figure, it is observed that $t_p$ is approximately directly proportional to $\lambda$. This conclusion is in agreement with that of the experimental curve, which is also presented in the figure.

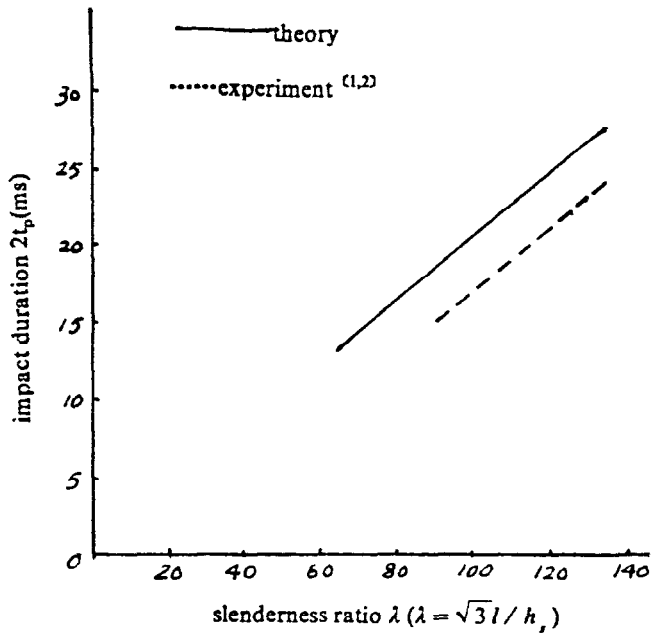


**Figure 5.** Relationship between peak impact time and slenderness ratio.

*Example 2. Calculation of the critical impact values*

Three impact criteria defining the structural elastic and inelastic behavior in fluid–structure impact buckling have been suggested in Refs. 1 and 2. The three criteria are buckling, plasticity, and plastic collapse. These criteria will be used in the numerical analysis. For convenience, they are restated as follows:

- buckling criterion—for a column with a prescribed slenderness, the fluid–structure impact buckling is identified as occurring in one impact if the peak axial compressive strain $\epsilon_c$ reaches a critical value $\epsilon_{c,erb}$ at which the maximum bending strain $|\epsilon_b|_{\max}$ grows to a value equal to the axial loading magnitude. $\epsilon_{c,erb}$ is called critical buckling impact strain.
- plasticity criterion—for a column with a prescribed slenderness, the fluid–structure impact plasticity is identified as occurring in one impact if $\epsilon_c$ reaches (does not exceed) a critical value $\epsilon_{c,ery}$ at which the maximum compressive-bending resultant strain $|\epsilon|_{\max}$ grows to a value equal to the yield strain of the material. $\epsilon_{c,ery}$ is called critical plasticity impact strain.
- collapse criterion—for a column with a prescribed slenderness, the fluid–structure impact plastic collapse is identified as occurring in one impact if $\epsilon_c$ reaches a critical value $\epsilon_{c,erf}$ beyond which further increases in drop height result in decreases in the peak axial loading strain rather than in increases. $\epsilon_{c,erf}$ is called critical plastic collapse impact strain.

Below, we will use the buckling and plasticity criteria for calculating the numerical results of the critical buckling and plasticity impact strains. The model cannot describe the column's plastic collapse; therefore the critical impact strain $\epsilon_{c,erf}$ cannot be calculated in this numerical analysis.

The columns used in this example are also those of s11, s21 and s31 in Refs. 1 and 2. The geometrical sizes of these columns are given in the previous example. The initial geometrical disturbance also takes the form of

**Table 1.** Numerical results for critical impact values.

| Specimen | Critical buckling impact value $\epsilon_{c,erb}(\mu$ strain) | | Critical plasticity impact value $\epsilon_{c,ery}(\mu$ strain) | |
|---|---|---|---|---|
| | Theory | Experiment[1,2] | Theory | Experiment[1,2] |
| s11 | 610.0 | 470.0 | 750.0 | 580.0 |
| s21 | 700.0 | 540.0 | 840.0 | 600.0 |
| s31 | 1100.0 | 820.0 | 1000.0 | 750.0 |

(22), except that $w_0$ is given by the real imperfections measured in the experiment.

To obtain the critical impact values, each of the columns considered is calculated under different impacts that correspond to different drop heights. The calculation for each impact gives a maximum compressive-bending resultant strain $|\epsilon|_{\max}$, maximum bending strain $|\epsilon_b|_{\max}$, and maximum compressive strain $|\epsilon_c|$. For different impacts, these results are drawn with two curves: $|\epsilon|_{\max}$ vs. $|\epsilon_c|$ and $|\epsilon_b|_{\max}$ vs. $|\epsilon_c|$. From these two curves and the buckling and plasticity criteria, the numerical results of $\epsilon_{c,erb}$ and $\epsilon_{c,ery}$ are determined. The numerical values of the three columns are presented in *Table 1* in which the experimental values are also listed for comparison. It is seen from the table that the discrepancies between the two sets of results range from 29% to 40%. This agreement is acceptable, even quite good, since in the present model we treat the air motion with the one-dimensional theory whereas in the experiment the motion of the air is two-dimensional flow.

## Conclusion

This paper presents a theoretical model for a coupled fluid–structure impact buckling phenomenon. The model is an impact system consisting of a small imperfection elastoplastic column with its upper end attached to a large mass and its lower end to a flat plate, an incompressible viscous water field, and a one-dimensional inviscid air layer lying between the plate and the water free surface. When the mass-column-plate unit in the system perpendicularly impacts the water free surface from a certain drop height or in a certain falling velocity, the column will produce a transversely flexural vibration due to the axial compression induced by the hydrodynamic slamming between the plate and the water. The flexural vibration simulates a coupled buckling phenomenon occurring in some fluid–structure impact environments where structural buckling is caused by fluid–structure impact and strongly depends on the hydrodynamic behavior of the fluid.

The paper provides a mathematical description for the model motion. In the description, the motion is divided into two phases. The first phase corresponds to $0 \le t \le t_p$ and the second phase to $t_p \le t \le t_0$ where $t_p$ is the peak impact time. For $0 \le t \le t_p$, the motion is treated as a coupling problem between the structural buckling and the hydrodynamic slamming. In this phase, the virtual work principle and the Prandtl–Reuss plastic theory are applied to the structural buckling, the one-dimensional continuity and momentum equations of a compressible inviscid fluid are applied to the air motion, and the two-dimensional Navier-Stokes equations of an incompressible viscous fluid are applied to the water motion. This phase ends when the deformed water free surface makes contact with the edge of the plate. In the second phase, the motion is treated as a decoupled structural buckling problem where the column is assumed to be loaded by a prescribed axial compression.

In numerical analysis for the first phase, the three sets of coupled equations are first decomposed by a staggered iteration method. The decoupled structural equation is then solved by a nonlinear finite element method with the Wilson-$\theta$ time integration scheme; the decoupled air and water equations are solved by a finite difference method. The paper calculates two numerical examples. One example is a calculation of the relationship between the column's slenderness and the slamming duration; the other is a calculation of the column's critical impact values. The numerical results are compared with the experimental ones and the agreement is found to be quite good.

## Nomenclature

| | |
|---|---|
| $u^c,u^b$ | column's membrane and bending displacements |
| $\chi^c,\chi^b$ | column's generalized membrane and bending strains |
| $N^c,N^b$ | column's membrane force and bending moment |
| $\sigma,\sigma_Y$ | column's stress and yield stress |
| $\xi,\eta$ | column's length and thickness coordinates |
| $\iota$,le | column's length and length in a finite element |
| $\lambda,A$ | column's slenderness and cross-section area |
| $E,H'$ | column's elastic modulus and strain-hardening parameter |
| $\rho_s,\rho_s^*$ | column's bulk and length densities, $\rho_s^* = \rho_s \cdot A$ |
| $M,m$ | point mass and mass of flat plate in Fig. 1 |
| $\beta_1,\beta_2$ | $\beta_1 = m/M$, $\beta_2 = 1/M$ |
| $a,b$ | half length and width of flat plate in Fig. 1 |
| $V,g$ | velocity of flat plate and gravity acceleration |
| $x,y$ | rectangular coordinates in air and water regions |
| $u_a,p_a$ | air velocity and pressure (absolute) |
| $p_{atm},\rho_{atm}$ | atmospheric pressure and density under $p_{atm}$ |

$h_a$,$h$ air layer thickness and height of deformed water region
$u$,$v$ water velocities in $x$ and $y$-directions
$u_s$,$v_s$ free-surface water velocities in $x$ and $y$-directions
$p$,$\rho$ water pressure (absolute) and density
$\mu$,$\nu$ water dynamic and kinematic viscosities
$h_m$, $L$ reference height and half width of water region
$t_o$,$t_p$ impact duration and peak impact time

## References


1 Zhang, Q. A coupled fluid–structure impact buckling-experiment and theory. Ph.D. Thesis, Huazhong University of Science and Technology, People's Republic of China, 1990
2 Zhang, Q., Li, S., and Zheng, J. Dynamic response, buckling and collapse of elasto-plastic straight columns under fluid-structure slamming compression. *Int. J. Solids Struct.* 1992, **29**(3), 381–397
3 Bolotin, V. V. *The Dynamic Stability of an Elastic System.* Holden-Day, San Francisco, 1964
4 Lindberg, H. E. and Florence, A. L. *Dynamic Pulse Buckling—Theory and Experiment.* Kluwer Academic Publishers, Amsterdam, 1987
5 Simitses, G. J. Stability of dynamic-loaded structures. *Appl. Mech. Rev.* 1987, **40**(10), 1403–1408
6 Owen, D. R. J. and Hinton, E. *Finite Element in Plasticity: Theory and Practice.* Pineridge Press Limited, Swansea, U.K., 1983
7 Zhang, Q., Li, S., and Zheng, J. Nonlinear dynamic behavior of stiffened plate under instantaneous loading. *Comput. Struct.* 1991, **40**(6), 1351–1356
8 Chuang, S. L. Experiments on flat-bottom slamming. *J. Ship Res.* 1966, **10**, 10–17
9 Chuang, S. L. Investigation of impact of rigid and elastic bodies with water. Rept. No. 3248, Naval Ship Research and Development Center, Washington, D.C., Feb. 1970, 110 pp.
10 Verhagen, J. H. G. The impact of a flat-plate on a water surface. *J. Ship Res.* 1967, **11**(4), 211–223
11 Koehler, Jr., B. R. and Kettleborough, C. F. Hydrodynamic impact of a falling body upon a viscous incompressible fluid. *J. Ship Res.* 1977, **21**(3), 165–181
12 Bathe, K. J. and Wilson, E. L. *Numerical Methods in Finite Element Analysis.* Prentice-Hall, Englewood Cliffs, N.J., 1976
13 Wilson, E. L. Nonlinear dynamic analysis of complex structures. *E.E.S.D.* 1973, **1**, 224–252